Molecular Genetic Dissection of Mouse Unconventional Myosin-VA: Tail Region Mutations

Jian-Dong Huang,* Valerie Mermall,† Marjorie C. Strobel,* Liane B. Russell, Mark S. Mooseker,†,‡,§ Neal G. Copeland* and Nancy A. Jenkins***

Manuscript received September 19, 1997
Accepted for publication December 23, 1997

**ABL-Basic Research Program, NCI-Frederick Cancer Research and Development Center, Frederick, Maryland 21702, †Department of Biology, ‡Department of Pathology, §Department of Cell Biology, Yale University, New Haven, Connecticut 06520 and **Oak Ridge National Laboratory, Oak Ridge, Tennessee 37831*

ABSTRACT

We used an RT-PCR-based sequencing approach to identify the mutations responsible for 17 viable *dilute* alleles, a mouse-coat-color locus encoding unconventional myosin-VA. Ten of the mutations mapped to the MyoVA tail and are reported here. These mutations represent the first extensive collection of tail mutations reported for any unconventional mammalian myosin. They identify sequences important for tail function and identify domains potentially involved in cargo binding and/or proper folding of the MyoVA tail. Our results also provide support for the notion that different myosin tail isoforms produced by alternative splicing encode important cell-type-specific functions.

ONE of the best-studied classes of unconventional myosins is myosin-V (MyoV). MyoV is evolutionarily well conserved and *Myo5*-related genes have been identified in multiple different organisms (Mooseker and Cheney 1995; Hasson and Mooseker 1996). Class V myosins include mouse and human MyoVA (Mercer *et al.* 1991; Engle and Kennett 1994; Moore *et al.* 1995; Zhao *et al.* 1996) and mouse and rat MyoVB (Hasson *et al.* 1996; Zhao *et al.* 1996), chicken brain MyoVA (p190) (Espreafico *et al.* 1992; Sanders *et al.* 1992), and yeast MYO2 (Johnston *et al.* 1991) and MYO4 (Haarer *et al.* 1994). Class V myosins have been shown to function as actin-based molecular motors in several different motility assays and move toward the barbed ends of actin filaments (Cheney *et al.* 1993). Purification of MyoVA from chicken brain has allowed the visualization of individual molecules by electron microscopy. As predicted from sequence data, MyoVA forms a two-headed molecule attached to a stalk that ends in a globular structure believed to represent the terminal ~400 amino acid domain (Cheney *et al.* 1993). This C-terminal domain is generally conserved among family members, suggesting that it encodes a conserved function(s).

Studies in both yeast and vertebrates have been very informative with respect to the function of MyoV family members. The yeast MYO2 gene was identified in a screen for temperature-sensitive cell division cycle mutations and is essential for cell survival (Johnston *et al.* 1991). At the restrictive temperature, the *myo2-66* mutation produces unbudded, enlarged cells with accumulated secretory vesicles. The MYO2 protein concentrates in regions of active growth, as caps at incipient bud sites and on small buds, at the mother-bud neck just before cell separation, and in mating cells as caps on shmoo tips and at the fusion bridge of zygotes (Lillie and Brown 1994). This phenotype has led to the suggestion that MYO2 is involved in organelle trafficking or membrane targeting. Hiu *et al.* (1996) demonstrated a requirement for MYO2 in vacuolar inheritance in yeast.

MYO4 is important for mating-type switching in yeast (Jansen *et al.* 1996). Cells of budding yeast give birth to mother and daughter cells that differ in that only mother cells express the HO endonuclease gene and thereby switch mating types. MYO4 is one of five cytoplasmic genes identified in a genetic screen that are required for mother-specific HO expression (Jansen *et al.* 1996). MYO4 is not, however, a mother-specific protein. On the contrary, MYO4 accumulates in growing buds. MYO4 apparently functions by transporting factors into the bud that repress HO expression such as the recently identified zinc finger protein ASH1 (Jansen *et al.* 1996).

In the mouse, MyoVA is encoded by the *dilute* locus (Mercer *et al.* 1991). Studies of *dilute* mice have suggested that mouse MyoVA is important for melanosome transport in melanocytes and transport of smooth endoplasmic reticulum in cerebellar Purkinje cell dendritic spines (Dekker-Ohno *et al.* 1996; Provance *et al.* 1996; Takagishi *et al.* 1996; Wu *et al.* 1997).

In an accompanying manuscript (Huang *et al.* 1998) we used an RT-PCR-based sequence approach to identify the mutations responsible for 17 viable, presumably

Corresponding author: Nancy A. Jenkins, ABL-Basic Research Program, P.O. Box B, Bldg. 539, Frederick, MD 21702-1201.
E-mail: jenkins@ncifcrf.gov

hypomorphic, *dilute* alleles. Ten of the mutations mapped to the MyoVA tail and are reported here. These mutations represent the first extensive collection of tail region mutations described for any unconventional mammalian myosin and provide interesting insights into tail region function.

MATERIALS AND METHODS

Mice: Seven of the alleles reported in this study were generated by mutagenesis of (101/Rl × C3H/Rl) F_1 hybrid mice, six at the Oak Ridge National Laboratory, Oak Ridge, TN (*Myo5a*^{34DENUg}, *Myo5a*^{2ENUR}, *Myo5a*^{5ENURg}, *Myo5a*^{6PXENURg}, *Myo5a*^{34ENURg}, and *Myo5a*^{33ENURf}) and one at the Medical Research Council Radiobiology Unit, Harwell, UK (*Myo5a*$^{d\text{-}105H}$). The remaining mutations arose spontaneously at The Jackson Laboratory, Bar Harbor, ME. The chromosomes of origin for these spontaneous alleles are as follows: C57BL/6J, *Myo5a*$^{d\text{-}J}$; C57BL/10SnJ, *Myo5a*$^{d\text{-}n}$; and C57BL/6J, *Myo5a*$^{d\text{-}n2J}$. Two mutations, *Myo5a*^{2ENUR} and *Myo5a*^{33ENURf}, are extinct and all analyses were performed on frozen tissues. The remaining eight mutations are maintained at the National Cancer Institute-Frederick Cancer Research and Development Center, Frederick, MD. With the exception of *Myo5a*$^{d\text{-}n2J}$, all mutations are propagated in the homozygous condition. *Myo5a*$^{d\text{-}n2J}$ mice are maintained by crossing carriers to C57BL/6J-*d*^{v} *se*/*d*^{v} *se* mice.

Northern analysis, protein analysis, and RT-PCR sequencing were done as described in Huang *et al.* (1998).

RESULTS

We have used an RT-PCR-based sequencing approach to identify the mutations responsible for 17 viable *dilute* mutations that vary in their effect on coat color and the nervous system. Seven of the mutations mapped to the MyoVA head and are reported in an accompanying manuscript (Huang *et al.* 1998). Ten of the mutations mapped to the MyoVA tail and are described here (Table 1; Figure 1). None of the mutations mapped to the MyoVA neck. This may reflect the small target size of the neck. Alternatively, only viable mutations were sequenced in these studies, and it is possible that neck mutations are primarily homozygous lethal because of the importance of this region in light-chain binding and subsequent regulation of MyoVA activity.

Among the 10 tail mutations, seven affect only coat color: one is a *d* mutation, which when homozygous results in a lightened coat, and six are *d*^{x} mutations, which when homozygous cause a coat color intermediate in phenotype between wild-type and *d* mice. The remaining three mutations, which are designated *d*^{n}, cause a lightened coat (similar to *d*) and have a neurological disorder of varying severity (Table 1). No *d*^{xn} mutations, that is, *d*^{x} in color in combination with a neurological disorder, were identified in the tail. This was surprising given that three of seven head region mutations were from the *d*^{xn} class (Huang *et al.* 1998). This paucity of *d*^{xn} mutations may reflect an inherent difficulty in generating this class of alleles via mutations in the tail. Alternatively, it may simply be due to random chance.

Five of the tail mutations were induced by ethylnitrosourea (ENU) (*Myo5a*^{5ENURg}, *Myo5a*^{34DENUg}, *Myo5a*^{2ENUR}, *Myo5a*^{34ENURg}, and *Myo5a*^{33ENURf}) (Table 1). The vast majority of germline ENU-induced mutations characterized

TABLE 1

Tail region mutations

Mutant class	Allele name	Phenotype[a]		Mutagen[b]	Percent *Myo5a* RNA levels[c]	Percent MyoVA protein levels[d]	Mutation
		Pigment dilution	Neurological impairment				
d^{x}	*Myo5a*^{5ENURg}	+	0	ENU	77	2	T4578A, M1513K
d^{x}	*Myo5a*^{34DENUg}	++	0	ENU	65	13	T3672A, L1211Q
d^{x}	*Myo5a*$^{d\text{-}105H}$	++	0	R	95 (100)	39	G→T, Splice
d^{x}	*Myo5a*^{2ENUR}	++	0	ENU	110 (100)	84	A→G, Splice
d^{x}	*Myo5a*^{6PXENUe}	++	0	R+ENU	92	4	A4596G, D1519G
d^{x}	*Myo5a*^{34ENURg}	++	0	ENU	45 (80)	25	T→C, Splice
d	*Myo5a*$^{d\text{-}J}$	++++	0	S	7	<1	Deletion
d^{n}	*Myo5*^{a33ENURf}	++++	+	ENU	103	4	T4569A, I1510N
d^{n}	*Myo5a*$^{d\text{-}n}$	++++	+	S	91	<1	C5558T, Q1840Stop
d^{n}	*Myo5a*$^{d\text{-}n2J}$	++++	+++	S	12 (0)	<1	G→T, Splice

[a] The relative severity of the phenotype of the various alleles with respect to coat color and neurological behavior has been estimated; it ranges from unaffected (wild type), indicated by 0, to extreme, indicated by ++++. All radiation and ENU mutations were induced in spermatogonial stem cells.

[b] ENU, ethylnitrosourea; S, spontaneous; R, radiation.

[c] Percent wild-type control brain RNA levels. The numbers in parentheses represent the percent *Myo5a* mutant brain RNA that is correctly spliced. Note that the *Myo5a*$^{d\text{-}105}$ and *Myo5a*^{2ENUR} splicing mutations do not affect the *Myo5a* splice form expressed in brain.

[d] MyoVA brain protein levels were quantitated relative to MyoVI using a MyoVA head region antibody.

to date are caused by A:T to G:C transitions (50%) or A:T to T:A transversions (36%) (reviewed in Marker *et al.* 1997). The same is true for the ENU-induced tail mutations where 40% (two of five) were caused by A:T to G:C transitions and 60% (three of five) by A:T to T:A transversions (Table 1).

The five other mutations mapping to the tail are either spontaneous (three), X-ray-induced (one), or induced by a combination of X-irradiation and ENU mutagenesis (one) (Table 1). The three spontaneous mutations, *Myo5a*$^{d\text{-}J}$, *Myo5a*$^{d\text{-}n}$, *Myo5a*$^{d\text{-}n2J}$, were caused by a genomic deletion, a missense mutation, or a splicing mutation, respectively (Table 1). All three types of lesions have been commonly associated with spontaneous mouse germline mutations (summarized in Bedell *et al.* 1997). The X-ray-induced mutation, *Myo5a*$^{d\text{-}105H}$, was caused by a splicing mutation resulting from a G to T transversion (Table 1). Although X-ray-induced mutations are usually associated with large genomic deletions, inversions, or other complex rearrangements, a few X-ray-induced mutations have been associated with point mutations (Marker *et al.* 1997). *Myo5a*^{6PXENUe} was found in the offspring of an (101/Rl × C3H/Rl) F_1 male that had received 300r X-rays five days prior to being injected with 100 mg/kg ENU. The *Myo5a*^{6PXENUe} mutation was caused by a missense mutation resulting from an A4596G transition. As ~50% of all ENU-induced mutations are caused by A:T to G:C transitions, it seems most likely that the *Myo5a*^{6PXENUe} mutation was induced by ENU. In support of this notion is the observation that *Myo5a*^{6PXENUe} was induced in spermatogonial stem cells in which 100 mg ENU/kg are more mutagenic than are 300r X rays (Russell 1965; Russell *et al.* 1982). In light of this conclusion, we have recalculated the number of transitions and transversions observed in the ENU-induced alleles and find that it is 50% for each class.

MyoVA mRNA and protein expression levels: To determine if any of the tail mutations affected *Myo5a* mRNA expression levels, brain RNA from each of the 10 mutations was characterized by Northern analysis (Figure 2) and *Myo5a* mRNA levels were quantitated relative to a wild-type control (Table 1). *Myo5a* mRNA levels were as follows: not significantly altered by five mutations, *Myo5a*$^{d\text{-}105H}$, *Myo5a*^{2ENUR}, *Myo5a*^{6PXENUe}, *Myo5a*^{33ENURf} and *Myo5a*$^{d\text{-}n}$; moderately reduced by three mutations, *Myo5a*^{5ENURg}, *Myo5a*^{34DENUg}, and *Myo5a*^{34ENURg}; and severely reduced by two mutations, *Myo5a*$^{d\text{-}J}$ and *Myo5a*$^{d\text{-}n2J}$.

To determine if any of the mutations affected MyoVA protein levels, extracts from mutant brain were characterized by Western analysis using antibodies directed against the MyoVA head (Figure 3) and the levels quantitated relative to an internal MyoVI control (Table 1). Protein levels were severely reduced by seven muta-

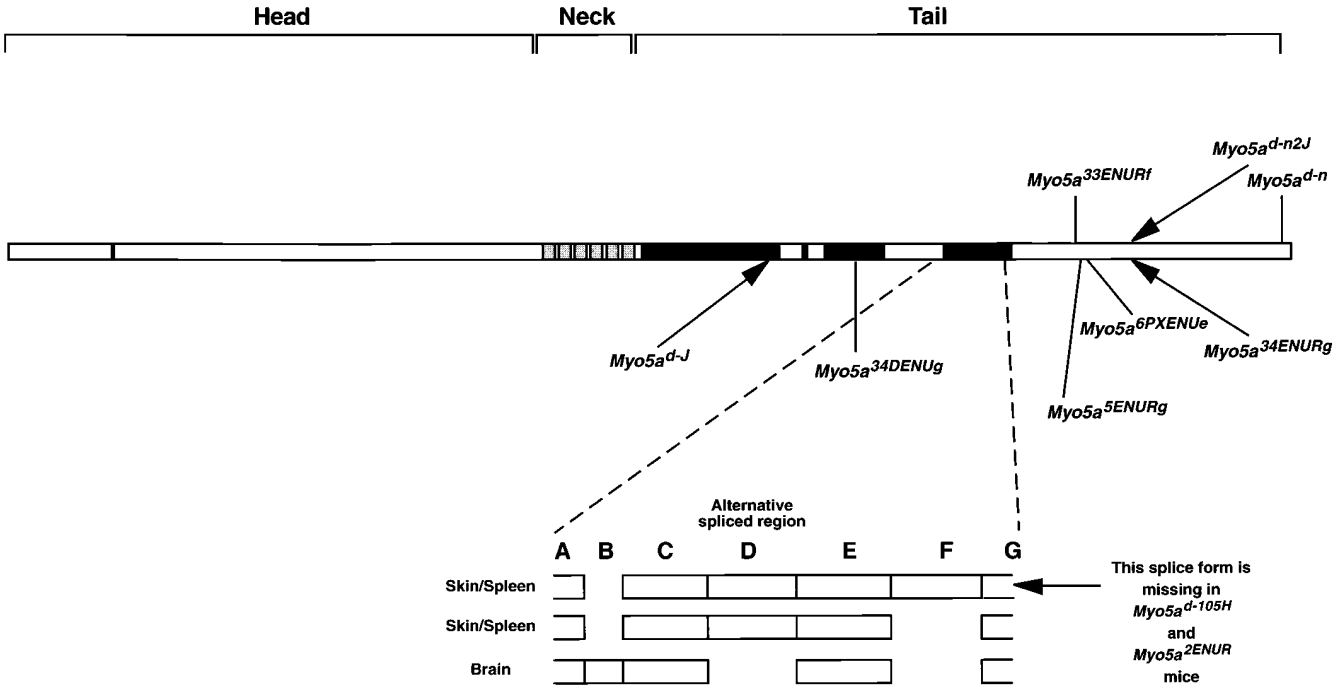

Figure 1.—Schematic representation of MyoVA showing the approximate location of the MyoVA tail-region mutations. The different functional domains of MyoVA, including the head, neck and tail, are indicated. The ATP-binding site and PEST regions are indicated by black rectangles, the IQ motifs by light gray rectangles, and coiled-coil domains by dark gray rectangles. Mutations below the schematic affect only coat color whereas mutations above the schematic affect both coat color and the nervous system. Splicing mutations are indicated by arrows. Exons encoding the different alternative MyoVA tail isoforms are indicated at the bottom of the figure.

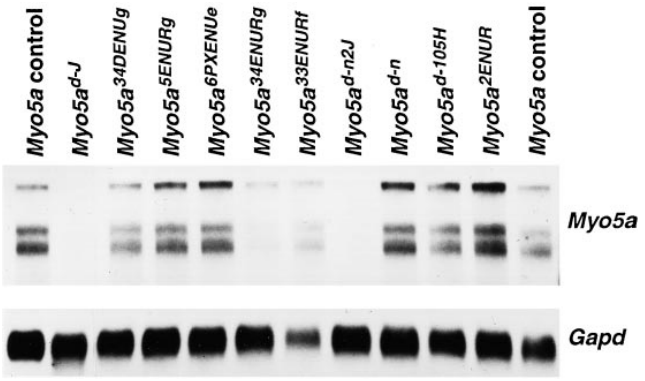

Figure 2.—Northern blot analysis of *Myo5a* mRNA levels from brain of homozygous viable *dilute* mutant mice. The three principal 7-, 8-, and 12-kb *Myo5a* transcripts are shown. RNA from C57BL/6J wild-type brain was used as control. *Gapd* (1.35 kb) was used as a loading control.

tions, *Myo5a*^{5ENURg}, *Myo5a*^{34DENUg}, *Myo5a*^{6PXENUe}, *Myo5a*$^{d-J}$, *Myo5a*^{33ENURf}, *Myo5a*$^{d-n}$, and *Myo5a*$^{d-n2J}$, and moderately reduced by two others, *Myo5a*$^{d-105H}$ and *Myo5a*^{34ENURg}. Similar to what was seen for the head region mutations (Huang *et al.* 1998), the reduction in protein levels was proportional to the severity of the mutant phenotype in only a few cases, such as *Myo5a*$^{d-n}$ and *Myo5a*$^{d-n2J}$ (Table 1). In contrast, the mildest allele in all of these studies, *Myo5a*^{5ENURg}, produces only 2% wild-type protein, and yet there is barely an effect on pigmentation (Table 1).

Mutations in the coiled-coil domain of the tail: Two of the *Myo5a* mutations, *Myo5a*$^{d-J}$ and *Myo5a*^{34DENUg}, mapped to the coiled-coil domain of the tail that is involved in protein dimerization (Figure 1). The *Myo5a*$^{d-J}$ mutation is unique in these studies in that *Myo5a*$^{d-J}$ animals display the full mutant phenotype in the coat but are neurologically normal (Table 1). A combination of RNA and genomic sequence analysis indicated that the *Myo5a*$^{d-J}$ mutation results from an ~1-kb genomic deletion that removes 8 bp of coding sequence from the first coiled-coil domain (Figure 4A). Because a splice acceptor site is removed by the deletion, no wild-type *Myo5a* transcripts are expressed in *Myo5a*$^{d-J}$ mice. Three mutant splicing products, however, were detected following RT-PCR amplification and cloning of *Myo5a*$^{d-J}$ brain mRNA. These transcripts were generated using cryptic splice acceptor sites located in both intron as well as exon sequence (Figure 4A). Two of these mutant transcripts, the 12-bp deletion and the 114-bp deletion, are in frame. Because *Myo5a*$^{d-J}$ mice are neurologically normal it would appear that at least one of these mutant proteins is functional in brain.

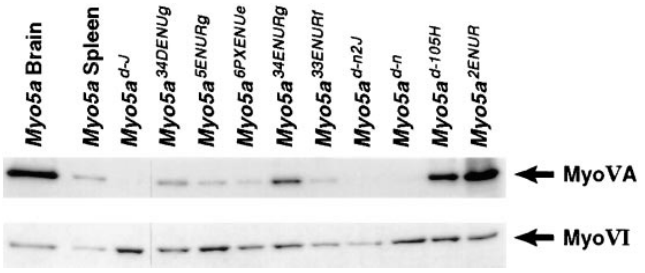

Figure 3.—Western blot analysis of MyoVA protein levels from brain of homozygous viable *dilute* mutant mice. Extracts from mutant brain as well as wild-type brain and spleen were probed with a MyoVA head region antibody. MyoVI was used as a loading control.

The *Myo5a*^{34DENUg} mutation results from a T3672A transversion that introduces an L1211Q substitution into the second coiled-coil domain (Table 1, Figure 1). Computer analysis using MacVector 6.0.1, Protein Analysis Toolbox, indicates that the coiled-coil structure is not disrupted by this substitution, which is consistent with the mild d^x phenotype caused by this allele. However, this mutation does appear to destabilize the protein and possibly the mRNA as well (Table 1).

Mutations in other regions of the tail: *Tissue-specific splicing mutations:* Three alternative splice forms of the MyoVA tail can be identified by PCR amplification and agarose gel electrophoresis (Figure 5). Splice form #3 is unique to brain. Splice forms #1 and #2 are seen in most other tissues, although their relative expression levels vary from tissue to tissue. Two mutations, *Myo5a*$^{d-105H}$ and *Myo5a*^{2ENUR}, map to this alternatively spliced region and specifically affect splice form #1. The *Myo5a*$^{d-105H}$ mutation results from a G to T transversion in exon F (Figure 4B). As a result of this mutation exon F is skipped and splice form #1 is not expressed (Figure 5). Neither splice form #2 nor #3 is affected by the exon F mutation (Figure 5). A number of investigators have reported that exon sequence is important for splicing (Mardon *et al.* 1987; Helfman *et al.* 1988; Cooper and Ordahl 1989; Hampson *et al.* 1989; Katz and Skalka 1990; Fu *et al.* 1991; Cooper 1992; Steingrimsdottir *et al.* 1992; Watakabe *et al.* 1993). Exon mutations could affect splicing in at least two ways. First, they could disrupt elements recognized by the splicing machinery, such as factors regulating alternative splicing. Second, they could change the secondary structure of the pre-mRNA and either sequester or expose splice sites. The precise mechanism responsible for exon F skipping in this mutant remains to be determined.

The *Myo5a*^{2ENUR} mutation results from an A to G transition in the splice acceptor site for exon F (Figure 4C). Again, exon F is skipped and neither splice form #2 nor #3 is affected (Figure 5). This A residue is 100% conserved in all reported 3′ splice junctions (Penotti 1991). The effects of mutations at this residue, however, are variable. In some cases, little effect on RNA processing is observed, whereas in others no wild-type transcripts are made (Krawczak *et al.* 1992).

Although all cells contain a cytoskeleton, the cytoskeleton performs different roles and contains different components in different cell types. Tissue-specific alter-

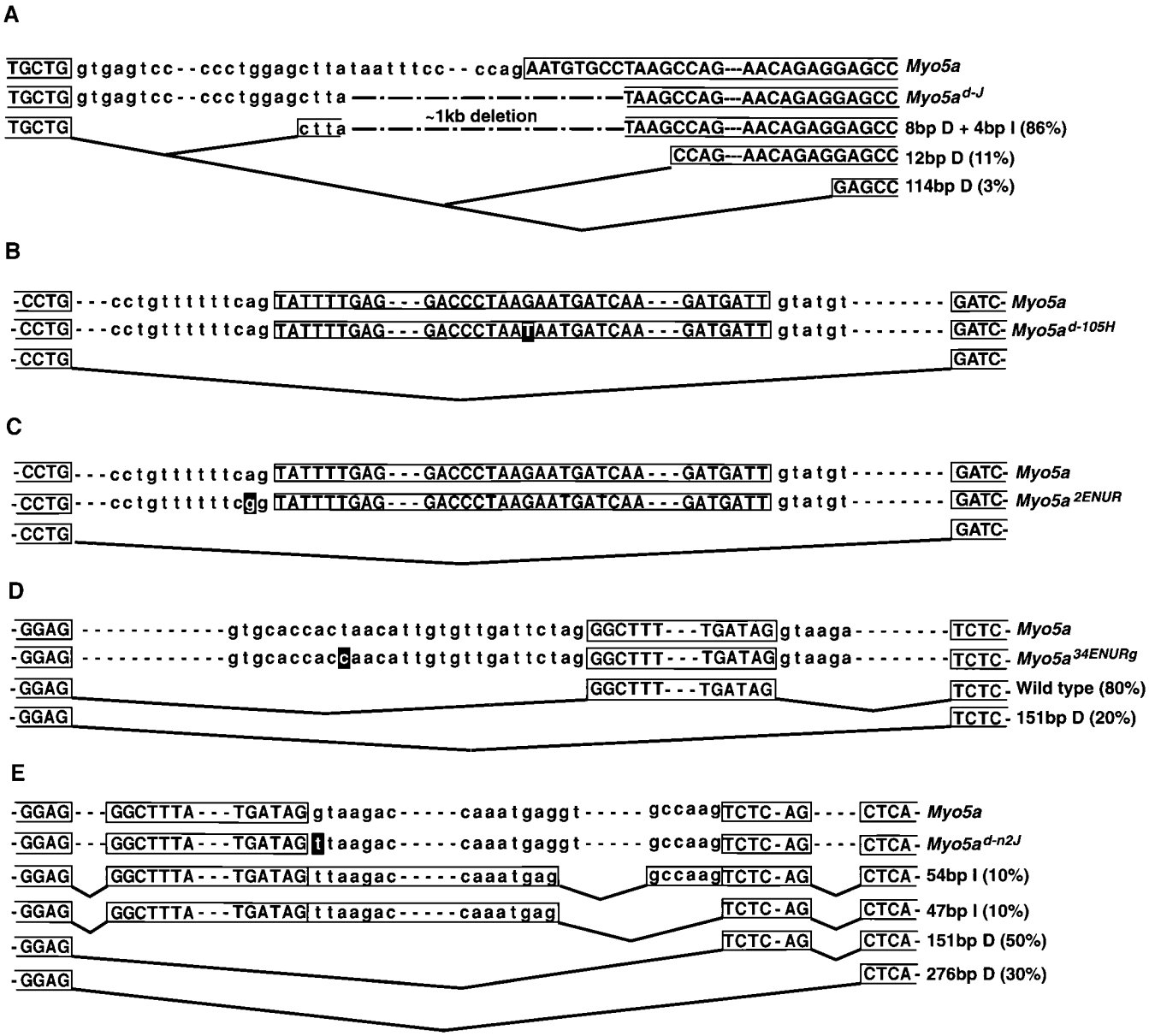

Figure 4.—*Myo5a* splicing mutations: genomic alterations and alternative splice products. Wild-type *Myo5a* genomic sequences are shown at the top of each panel followed by the corresponding mutant *Myo5a* genomic sequence. The different mutant splice products were determined by sequencing of agarose gel separated and/or cloned PCR amplification products. The relative abundance of the different splices, indicated in parentheses, was estimated by the number of clones obtained. At least 20 clones were analyzed for each mutant mouse. A deletion or insertion is indicated by letter D or I after the base pair change. Capital letters indicate exon sequence; lowercase letters indicate intron sequence. Dashes indicate noncontiguous sequence. Boxes represent cDNA sequences detected in these studies. (A) *Myo5a*$^{d\text{-}J}$ mutation. The first nucleotide shown at the far left is at position 3345 in the wild-type *Myo5a* cDNA; (B) *Myo5a*$^{d\text{-}105H}$, nucleotide 4195; (C) *Myo5a*^{2ENUR}, nucleotide 4195; (D) *Myo5a*^{34ENURg}, nucleotide 4756; (E) *Myo5a*$^{d\text{-}n2J}$, nucleotide 4756. The black rectangles shown in B–E represent the position and nature of the mutation.

native splicing is one way that a single cytoskeletal gene can produce many different proteins that perform different functions in different cell types. In the case of MyoVA, we have proposed that exon F might encode sequences necessary for MyoVA function in cells such as melanocytes and that exon B encodes sequences important for MyoVA function in the nervous system (Seperack *et al.* 1995). Consistent with this model, *Myo5a*$^{d\text{-}105H}$ and *Myo5a*^{2ENUR} mice are neurologically normal; only the coat color is affected by these two mild d^x mutations (Table 1).

Non-tissue-specific splicing mutations: Two additional splicing mutations, *Myo5a*^{34ENURg} and *Myo5a*$^{d\text{-}n2J}$, were localized to the MyoVA tail (Figure 1). Neither mutation is tissue-specific: all forms of the protein are equally affected by these two mutations. Two classes of *Myo5a*

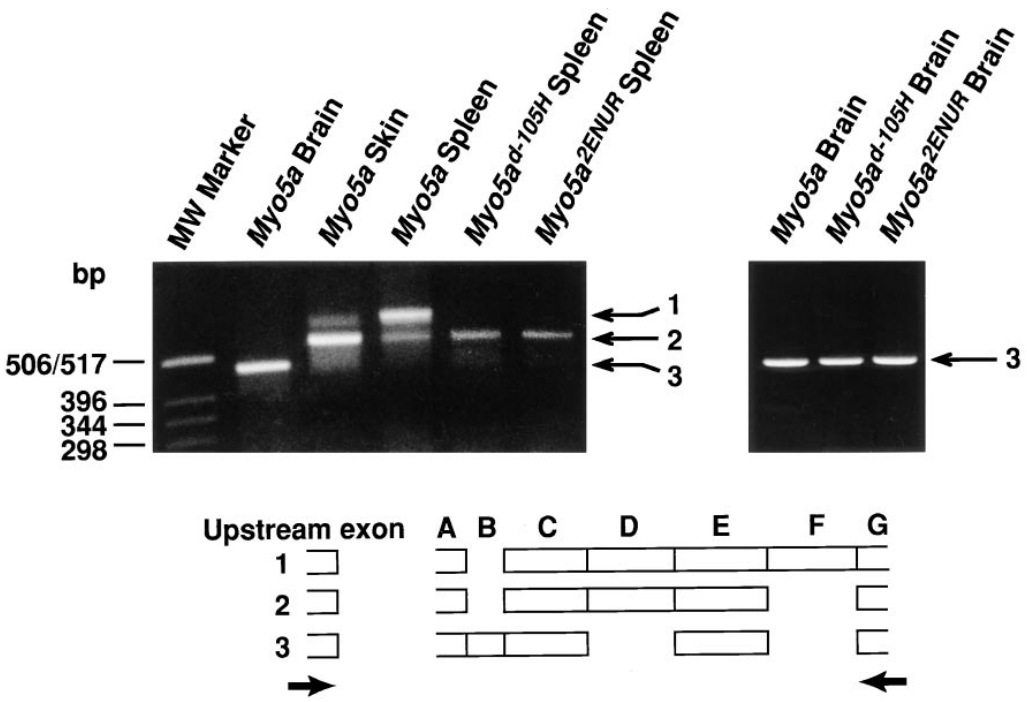

Figure 5.—Tissue specific splicing mutations. The different alternative splice forms of *Myo5a* were amplified by PCR. The structure of the three alternative splice forms of *Myo5a* are shown at the bottom of the figure. The capital letters represent exons as described previously (Seperack *et al.* 1995). The bold arrows represent the primer set used in RT-PCR amplification. An agarose gel containing the wild-type *Myo5a* amplification products from brain, skin, and spleen together with products from $Myo5a^{d\text{-}105H}$ and $Myo5a^{2ENUR}$ spleen is shown at the left of the figure. Products from $Myo5a^{d\text{-}105H}$ and $Myo5a^{2ENUR}$ brain are shown at the right of the figure. The sequence of spliced forms #1 through #3 of both wild-type and mutant mice was determined by direct sequencing after gel purification of each amplified fragment.

transcripts are expressed in $Myo5a^{34ENURg}$ mice. One class is wild type and the other class contains a 151-bp out-of-frame deletion (Figure 4D). Genomic sequence analysis showed that the 151-bp deletion results from exon skipping because of a T to C transition in the polyprimidine tract located upstream of the skipped exon (Figure 4D). As expected from the subtle nature of this mutation, as much as 80% of the *Myo5a* mRNA expressed in $Myo5a^{34ENURg}$ mice is normally spliced. No truncated protein was detected by Western analysis (Figure 3) and wild-type protein was made at ~25% normal levels (Table 1). These results are consistent with the subtle d^x phenotype of $Myo5a^{34ENURg}$ mice.

$Myo5a^{d\text{-}n2J}$ is the most severe neurological mutation localized to the tail region. Like d^J mice, these mice are neurologically impaired by 14–21 days after birth. However, instead of dying from these neurological defects as mice homozygous for the d^J alleles do, mice homozygous for $Myo5a^{d\text{-}n2J}$ show some improvement as they age and can be kept alive for extended periods of time. Northern and Western blot analysis showed only 12% of the normal *Myo5a* RNA level and <1% of the normal MyoVA protein level in $Myo5a^{d\text{-}n2J}$ brain (Table 1, Figures 2 and 3). Four abnormal classes of *Myo5a* transcripts were detected in $Myo5a^{d\text{-}n2J}$ brain (Figure 4E). Two classes carried deletions and two carried insertions relative to wild-type transcripts. Genomic sequence analysis indicated that these abnormal transcripts resulted from a G to T transversion in a conserved GT splice donor consensus sequence (Figure 4E). Because the G is absolutely conserved in all GT splice donor consensus sequences, it is not surprising that wild-type *Myo5a* transcripts are not detected in these mice. Only two of the abnormal splices are in-frame, the 54-bp insertion and the 276-bp deletion. Although both transcripts could theoretically encode functional protein, it seems unlikely that a protein with a 92 amino acid deletion in the tail region would be functional. Presumably, however, at least one of the proteins must retain some function as homozygous $Myo5a^{d\text{-}n2J}$ mice are viable.

Clustered missense mutations: Three of the globular tail region mutations were missense mutations (Table 1). Interestingly, all three mutations are located within 10 amino acids of each other (Figure 1, Table 1). $Myo5a^{33ENURf}$ results from an I1510N substitution; $Myo5a^{5ENURg}$, a M1513K substitution; and $Myo5a^{6PXENUe}$, a D1519G substitution. None of the mutations significantly affect *Myo5a* mRNA levels, but all produce fairly dramatic reductions in MyoVA protein levels (2–4% wild-type levels) (Table 1). However, these reduced protein levels do not correlate well with the severity of the phenotypes. As mentioned previously, the $Myo5a^{5ENURg}$ mutation produces a very subtle change in color yet makes only 2% wild-type protein. Both $Myo5a^{6PXENURg}$ and $Myo5a^{33ENURf}$ produce 4% wild-type protein but $Myo5a^{33ENURf}$ has a much more severe effect on pigmentation than the other two alleles, and it also affects the nervous system (Table 1).

A protein truncation mutation: The $Myo5a^{d\text{-}n}$ mutation

results from a C5558T transition that introduces a stop codon at residue 1840 of the protein (Figure 1, Table 1). Fourteen amino acid residues are deleted from the end of the mature MyoVA protein by this mutation. *Myo5a* mRNA levels are not significantly affected in *Myo5a*$^{d\text{-}n}$ mice (91%); however, MyoVA protein levels are dramatically reduced (<1%) (Table 1). *Myo5a*$^{d\text{-}n}$ is similar to the *Myo5a*^{33ENURf} mutation with respect to both color and neurological abnormalities. At 14–21 days after birth the mutant animals are as neurologically impaired as d^{l} mice. However, as they age they recover completely and as adults are neurologically normal. A number of explanations could account for this phenotype in *Myo5a*$^{d\text{-}n}$ mice. For example, the 14 amino acids deleted by this mutation could encode residues important for MyoVA function in young animals but not in the adult, at least with respect to the nervous system. Alternatively, the phenotype of *Myo5a*$^{d\text{-}n}$ mice may be explained by the very low MyoVA protein levels (<1%) seen in *Myo5a*$^{d\text{-}n}$ mice. Perhaps higher MyoVA protein levels are required within the first few weeks after birth when the nervous system is still developing as compared to older animals, in which the nervous system is fully developed.

DISCUSSION

In studies reported here we describe 10 mutations that map to the coiled-coil or globular domains of the tail region of unconventional mouse MyoVA. These mutations represent the first extensive collection of tail region mutations described for any unconventional myosin. Although a large number of mutations have been reported for another unconventional myosin, *Myo7a*/*MYO7A* (Gibson *et al.* 1995; Weil *et al.* 1995; Weston *et al.* 1996; Levy *et al.* 1997; Liu *et al.* 1997), only two missense mutations have been mapped to the *MYO7A* tail (Levy *et al.* 1997). One mutation is located in the C-terminal Ezrin-Radixin-Moesin (ERM) domain that is conserved in band 4.1 superfamily members. The presence of the mutation may impair binding of the MYOVIIA ERM domain to its putative ligand. The other mutation lies 20 amino acids downstream of the α-helical domain, which is predicted to be involved in MYOVIIA dimerization.

Four of the 10 tail mutations were splicing mutations, five were missense mutations, and one resulted from an ~1-kb intragenic deletion. These results contrast with those for the head region mutations where all seven were missense mutations (Huang *et al.* 1998). The reason for this apparent difference is not clear. It does not appear to be because of the nature of the mutagen responsible for these mutations because all seven head region mutations were chemically induced as were two of four splicing mutations identified in the tail.

The *Myo5a* head mutations were roughly equally distributed along the length of the MyoVA head, and there was not obvious clustering of mutations with respect to phenotypic class, suggesting a simple model where the least severe amino acid changes correlate with the least severe *dilute* alleles (d^{x}), and the most severe are d^{xn} or d^{n} (Huang *et al.* 1998). With the exception of the two tissue specific splicing mutations, *Myo5a*$^{d\text{-}105H}$ and *Myo5a*^{2ENUR}, tail region results were consistent with this simple model.

The results for several tail region mutations suggest that the nervous system is relatively insensitive to the level of MyoVA protein. For example, mice homozygous for the *Myo5a*$^{d\text{-}J}$ mutation show a fully diluted coat color but are neurologically normal at all ages. The mutation is caused by a ~1-kb genomic deletion in the coiled-coil region, which decreases the level of protein in brain to <1% of that found in normal mice. Furthermore, none of the protein is wild type. Assuming that the region encompassed by the deletion is necessary for both melanocyte and neuron function, then a remarkably small amount of MyoVA is sufficient to rescue neurological phenotype. Furthermore, a nonsense mutation in *Myo5a*$^{d\text{-}n}$ mice results in the production of a 14 amino acid C-terminal truncated protein that is expressed at <1% of the level of that found in wild-type brain. Although *Myo5a*$^{d\text{-}n}$ mice are neurologically impaired when young, as adults they are normal and even breed in the homozygous condition.

Studies in both the *dilute* rat and the *dilute* mouse suggest that MyoVA is necessary for the transport of smooth endoplasmic reticulum (SER) to the dendritic spines of cerebellar Purkinje cells (Dekker-Ohno *et al.* 1996; Takagishi *et al.* 1996). Purkinje cell dendritic outgrowth begins shortly after birth, at a time when the neurological phenotype of *dilute* mice is first observed and is completed by 30 days of postnatal development (Ito 1984). The cerebellum is the major organ within the central nervous system involved in motor control, and the neurological defects observed in *dilute* mice are consistent with this SER defect. The phenotype of *Myo5a*$^{d\text{-}n}$ (as well as some of the other alleles that show improvement in neurological behavior with age) mice could reflect an increased need for MyoVA during postnatal development when Purkinje cell dendritic spines are being elaborated. Perhaps the low level of truncated MyoVA protein expressed in *Myo5a*$^{d\text{-}n}$ mice is sufficient for some SER transport, which rescues the lethality associated with *dilute* null alleles. Once dendritic outgrowth ceases in *Myo5a*$^{d\text{-}n}$ mice, SER transport could conceivably continue and eventually fill the empty dendritic spines that may have been produced during the neonatal growth of *Myo5a*$^{d\text{-}n}$ mice.

Two of the most informative tail region mutations were *Myo5a*$^{d\text{-}105H}$ and *Myo5a*^{2ENUR}. Both are tissue-specific splicing mutations that delete one of the three MyoVA splice forms. The splice form that is missing contains exon F, which is expressed in tissues such as spleen and skin but not in brain. This pattern of expression suggests

that exon F might encode sequences that allow MyoVA to carry different cargoes in tissues such as skin (melanocytes) and spleen versus brain (Purkinje cells). Consistent with this model, *Myo5a*$^{d\text{-}105H}$ and *Myo5a*^{2ENUR} mice are neurologically normal: only the coat color is mildly affected by these two mutations. In the future it will be interesting to perform yeast two-hybrid screens using tails as baits that either contain or lack exon F. Perhaps it will be possible to identify proteins expressed in tissues such as melanocytes that only bind baits carrying exon F.

Another region that may function in cargo binding is suggested by three mutations that cluster within 10 amino acids in the MyoVA tail, *Myo5a*^{33ENURf}, *Myo5a*^{5ENURg}, and *Myo5a*^{6PXENUe}. This clustering is not expected by random chance ($P < 1.6 \times 10^{-7}$), suggesting that an important functional domain of *Myo5a* may be located in this region of the tail. Interestingly, this 10 amino acid region is located 8 amino acids upstream from an ~280 amino acid C-terminal region that shares extensive sequence homology with two genes, *AF-6* and *cno* (Ponting 1995). *AF-6* was originally identified as the fusion partner for *ALL-1* in acute myeloid leukemias carrying the t(6;11) chromosome translocation (Prasad *et al.* 1993). *cno* is a *Drosophila melanogaster* gene thought to mediate interactions between the *Notch* signaling cascade and other signaling pathways (Miyamoto *et al.* 1995). What makes this homology interesting is that, in addition to the myosin homology, both *AF-6* and *cno* also share a region of homology with the kinesin-like molecule unc-104 (Ponting 1995). Like MyoVA, unc-104 has been proposed to function in anterograde transport within neurons (Hall and Hedgecock 1991). Although the function of the domains in *AF-6* and *cno* showing homology to kinesins and myosins is unknown, it has been proposed that when these domains are within intact motor proteins, they may mediate binding to cargo molecules and that, when within *AF-6* and *cno*, they may possess similar binding functions (Ponting 1995). Perhaps the three *Myo5a* mutations that are located near this *AF-6*/*cno* homology domain interfere with this cargo binding in melanocytes (*Myo5a*^{5ENURg} and *Myo5a*^{6PXENUe}) and melanocytes and neurons (*Myo5a*^{33ENURf}).

An alternative explanation for this clustering of mutations is that this region of the tail is important for protein folding. Consistent with this explanation, computer analysis (MacVector 6.0.1; Protein Analaysis Toolbox) predicts that all three mutations are not surface exposed and two of the mutations, *Myo5a*^{33ENURf} and *Myo5a*^{5ENURg}, are located in hydrophobic regions. The third mutation, *Myo5a*^{6PXENUe}, is predicted to be located at the border between a hydrophobic and hydrophilic region. In addition, all three mutations are predicted to increase the hydrophilicity of the protein. An effect on protein folding could also account for the protein instability that results from these three mutations.

Finally, recent studies have identified mutations in *MYOVA* in humans with Griscelli disease (Pastural *et al.* 1997). Griscelli disease is a rare autosomal recessive disorder characterized by pigment dilution, variable cellular immunodeficiency and onset of acute phases of uncontrolled lymphocyte and macrophage activation, leading to death in the absence of bone-marrow transplantation. The pigment defect in Griscelli patients is associated with clumping of pigment in the hair shaft and an accumulation of melanosomes within melanocytes similar to what is seen in *dilute* mice. However, unlike *dilute* mice, Griscelli disease has many features in common with the Chédiak-Higashi syndrome (CHS) including oculocutaneous albinism and immunodeficiency, as well as the occurrence of uncontrolled lymphoxyte/macrophage activation syndrome. CHS patients have defects in a gene called *LYST*, which is thought to play a role in vesicular transport and intracellular protein trafficking (Barbosa *et al.* 1996; Nagle *et al.* 1996). The phenotypic similarity between Griscelli and CHS patients suggests that LYST and MYOVA proteins may directly interact or function in the same intracellular trafficking pathway.

Two *MYOVA* mutations have been identified in Griscelli patients (Pastural *et al.* 1997). One mutation is in the coil-coil region of the tail and probably affects protein dimerization. The second mutation introduces a stop codon in front of the putative calmodulin/light chain-binding domain and likely represents a null allele. Interestingly, the patient with the stop codon has a severe neurological disorder, similar to the neuroectodermal melanolysosomal disease described by Elejalde *et al.* (1977); and the patient with the tail region mutation is neurologically normal. It thus appears that in humans, as in mice, only the more severe *MYOVA* mutations have a neurological phenotype. Human *MYOVA* null alleles are not always neurologically lethal, however, although some Griscelli patients have been reported to die from brain degeneration associated with cellular infiltration (Haraldsson *et al.* 1991; Hurvitz *et al.* 1993). It is possible that some other motor protein can compensate for the absence of MYOVA in the human, but not mouse, nervous system.

We thank Jo Peters and Bruce Cattanach (MRC Radiobiology Unit, Harwell, UK) for providing mice carrying the *Myo5a*$^{d\text{-}105H}$ allele and Linda Washburn and Hope Sweet (The Jackson Laboratory, Bar Harbor, ME) for providing mice carrying the *Myo5a*$^{d\text{-}J}$, *Myo5a*$^{d\text{-}n}$, and *Myo5a*$^{d\text{-}n2J}$ alleles. We are grateful to Deborah A. Swing and Marilyn Powers for their help with these studies. This research was supported by the National Cancer Institute, Department of Health and Human Services, under contract with ABL (N.G.C. and N.A.J.); a basic research grant from the Muscular Dystrophy Association and National Institutes of Health grant DK-25387 (M.S.M.); American Cancer Society postdoctoral fellowship PF-4316 to V.M.; and the Office of Health and Environmental Research, U.S. Department of Energy (under contract DE-AC05-96OR22464 with Lockheed Martin Energy Research Corp.) jointly with the National Institute of Environmental Health Sciences under Interagency Agreement No. 1-Y01-ES-50318-00.

LITERATURE CITED

Barbosa, M. D. F. S., Q. A. Nguyen, V. T. Tchernev, J. A. Ashley, J. C. Detter *et al.*, 1996 Identification of the homologous beige and Chediak-Higashi syndrome genes. Nature **382:** 262–265.

Bedell, M. A., D. A. Largaespada, N. A. Jenkins and N. G. Copeland, 1997 Mouse models of human disease. Part II: Recent progress and future directions. Genes Dev. **11:** 11–43.

Cheney, R. E., M. K. O'Shea, J. E. Heuser, M. V. Coelho, J. S. Wolenski *et al.*, 1993 Brain myosin-V is a two-headed unconventional myosin with motor activity. Cell **75:** 13–23.

Cooper, T. A., 1992 In vitro splicing of cardiac troponin T precursors. Exon mutations disrupt splicing of the upstream intron. J. Biol. Chem. **267:** 5330–5338.

Cooper, T. A., and C. P. Ordahl, 1989 Nucleotide substitutions within the cardiac troponin T alternative exon disrupt pre-mRNA alternative splicing. Nucleic Acids Res. **17:** 7905–7921.

Dekker-Ohno, K., S. Hayasaka, Y. Takagishi, S. Oda, N. Wakasugi *et al.*, 1996 Endoplasmic reticulum is missing in dendritic spines of purkinje cells of the ataxic mutant rat. Brain Res. **714:** 226–230.

Elejalde, B. R., A. Valencia, E. F. Gilbert, G. Marin, J. Molina *et al.*, 1977 Neuro-ectodermal melanolysosomal disease: an autosomal recessive pigment mutation in man. Am. J. Med. Genet. **3:** 65–80.

Engle, L. J., and R. H. Kennett, 1994 Cloning, analysis, and chromosomal localization of myoxin (MYH12), the human homologue to the mouse dilute gene. Genomics **19:** 407–416.

Espreafico, E. M., R. E. Cheney, M. Matteoli, A. A. Nascimento, P. V. De Camilli *et al.*, 1992 Primary structure and cellular localization of chicken brain myosin-V (p190), an unconventional myosin with calmodulin light chains. J. Cell. Biol. **119:** 1541–1557.

Fu, X. D., R. A. Katz, A. M. Skalka and T. Maniatis, 1991 The role of branchpoint and 3′-exon sequences in the control of balanced splicing of avian retrovirus RNA. Genes Dev **5:** 211–220.

Gibson, F., J. Walsh, P. Mburu, A. Varela, K. A. Brown *et al.*, 1995 A type VII myosin encoded by the mouse deafness gene shaker-1. Nature **374:** 62–64.

Haarer, B. K., A. Petzold, S. H. Lillie and S. S. Brown, 1994 Identification of MYO4, a second class V myosin gene in yeast. J. Cell Sci. **107:** 1055–1064.

Hall, D. H., and E. M. Hedgecock, 1991 Kinesin-related gene unc-104 is required for axonal transport of synaptic vesicles in C. elegans. Cell **65:** 837–847.

Hampson, R. K., L. La Follette and F. M. Rottman, 1989 Alternative processing of bovine growth hormone mRNA is influenced by downstream exon sequences. Mol. Cell. Biol. **9:** 1604–1610.

Haraldsson, A., C. M. Weemaes, J. A. Bakkeren and R. Happle, 1991 Griscelli disease with cerebral involvement. Eur. J. Pediatr. **150:** 419–422.

Hasson, T., and M. S. Mooseker, 1996 Vertebrate unconventional myosins. J. Biol. Chem. **271:** 16431–16434.

Hasson, T., J. F. Skowron, D. J. Gilbert, K. B. Avraham, W. L. Perry *et al.*, 1996 Mapping of unconventional myosins in mouse and human. Genomics **36:** 431–439.

Helfman, D. M., W. M. Ricci and L. A. Finn, 1988 Alternative splicing of tropomyosin pre-mRNAs in vitro and in vivo. Genes Dev. **2:** 1627–1638.

Huang, J.-D., M. Jamie, T. V. Cope, V. Mermall, M. C. Strobel *et al.*, 1998 Molecular genetic dissection of mouse unconventional myosin-VA: head region mutations. Genetics **148:** 1951–1961.

Hurvitz, H., R. Gillis, S. Klaus, A. Klar, F. Gross-Kieselstein *et al.*, 1993 A kindred with Griscelli disease: spectrum of neurological involvement. Eur. J. Pediatr. **152:** 402–405.

Jansen, R. P., C. Dowzer, C. Michaelis, M. Galova and K. Nasmyth, 1996 Mother cell-specific HO expression in budding yeast depends on the unconventional myosin myo4p and other cytoplasmic proteins. Cell **84:** 687–697.

Johnston, G. C., J. A. Prendergast and R. A. Singer, 1991 The Saccharomyces cerevisiae MYO2 gene encodes an essential myosin for vectorial transport of vesicles. J. Cell Biol. **113,** 539–551.

Katz, R. A., and A. M. Skalka, 1990 Control of retroviral RNA splicing through maintenance of suboptimal processing signals. Mol. Cell. Biol. **10:** 696–704.

Krawczak, M., J. Reiss and D. N. Cooper, 1992 The mutational spectrum of single base-pair substitutions in mRNA splice junctions of human genes: causes and consequences. Hum. Genet. **90:** 41–54.

Levy, G., F. Leviacobas, S. Blanchard, S. Gerber, D. Largetpiet *et al.*, 1997 Myosin VIIa gene—heterogeneity of the mutations responsible for usher syndrome type Ib. Human Molecular Genetics **6:** 111–116.

Lillie, S. H., and S. S. Brown, 1994 Immunofluorescence localization of the unconventional myosin, Myo2p, and the putative kinesin-related protein, Smy1p, to the same regions of polarized growth in Saccharomyces cerevisiae. J. Cell Biol. **125:** 825–842.

Liu, X. Z., J. Walsh, P. Mburu, J. Kendrick-Jones, M. J. T. V. Cope *et al.*, 1997 Mutations in the myosin VIIA gene cause non-syndromic recessive deafness. Nature Genet. **16:** 188–190.

Mardon, H. J., G. Sebastio and F. E. Baralle, 1987 A role for exon sequences in alternative splicing of the human fibronectin gene. Nucleic Acids Res. **15:** 7725–7733.

Marker, P. C., K. J. Seung, A. E. Bland, L. B. Russell and D. M. Kingsley, 1997 Spectrum of Bmp5 mutations from germline mutagenesis experiments in mice. Genetics **145:** 435–443.

Mercer, J. A., P. K. Seperack, M. C. Strobel, N. G. Copeland and N. A. Jenkins, 1991 Novel myosin heavy chain encoded by murine dilute coat colour locus. Nature **349:** 709–713.

Miyamoto, H., I. Nihonmatsu, S. Kondo, R. Ueda, S. Togashi *et al.*, 1995 Canoe encodes a novel protein containing a GLGF/DHR motif and functions with Notch and scabrous in common developmental pathways in Drosophila. Genes Dev. **9:** 612–625.

Moore, K. J., J. R. Testa, U. Francke, A. Milatovich, N. G. Copeland *et al.*, 1995 Cloning and regional assignment of the human myosin heavy chain 12 (MYH12) gene to chromosome band 15q21. Cytogenet. Cell Genet. **69:** 53–58.

Mooseker, M. S., and R. E. Cheney, 1995 Unconventional myosins. Ann. Rev. Cell. Dev. Biol. **11:** 633–675.

Nagle, D. L., M. A. Karim, E. A. Woolf, L. Holmgren, P. Bork *et al.*, 1996 Identification and mutation analysis of the complete gene for Chediak-Higashi syndrome. Nature Genet. **14:** 307–311.

Pastural, E., F. J. Barrat, R. Dufourcq-Lagelouse, S. Certain, O. Sanal *et al.*, 1997 Griscelli disease maps to chromosome 15q21 and is associated with mutations in the Myosin-Va gene. Nature Genet. **16:** 289–292.

Penotti, F. E., 1991 Human pre-mRNA splicing signals. J. Theor. Biol. **150:** 385–420.

Ponting, C. P., 1995 AF-6/cno: neither a kinesin nor a myosin, but a bit of both. Trends Biochem. Sci. **20:** 265–266.

Prasad, R., Y. Gu, H. Alder, T. Nakamura, O. Canaani *et al.*, 1993 Cloning of the ALL-1 fusion partner, the AF-6 gene, involved in acute myeloid leukemias with the t(6;11) chromosome translocation. Cancer Res. **53:** 5624–5628.

Provance, D. W. Jr., M. Wei, V. Ipe and J. A. Mercer, 1996 Cultured melanocytes from dilute mutant mice exhibit dendritic morphology and altered melanosome distribution. Proc. Natl. Acad. Sci. USA **93:** 14554–14558.

Russell, W. L., 1965 Studies in mammalian radiation genetics. Nucleonics **23:** 53–56.

Russell, W. L., P. R. Hunsicker, G. D. Raymer, M. H. Steele, K. F. Stelzner *et al.*, 1982 Dose-response curve for ethylnitrosourea-induced specific-locus mutations in mouse spermatogonia. Proc. Natl. Acad. Sci. USA **79:** 3589–3591.

Sanders, G., B. Lichte, H. E. Meyer and M. W. Kilimann, 1992 cDNA encoding the chicken ortholog of the mouse dilute gene product. Sequence comparison reveals a myosin I subfamily with conserved C-terminal domains. FEBS Lett. **311:** 295–298.

Seperack, P. K., J. A. Mercer, M. C. Strobel, N. G. Copeland and N. A. Jenkins, 1995 Retroviral sequences located within an intron of the dilute gene alter dilute expression in a tissue-specific manner. EMBO J. **14:** 2326–2332.

Steingrimsdottir, H., G. Rowley, G. Dorado, J. Cole and A. R. Lehmann, 1992 Mutations which alter splicing in the human hypoxanthine-guanine phosphoribosyltransferase gene. Nucleic Acids Res. **20:** 1201–1208.

Takagishi, Y., S. Oda, S. Hayasaka, K. Dekker-Ohno, T. Shikata *et al.*, 1996 The *dilute-lethal* (d^l) gene attacks a Ca2+ store in the dendritic spine of Purkinje cells in mice. Neurosci. Lett. **215:** 169–172.

Watakabe, A., K. Tanaka and Y. Shimura, 1993 The role of exon sequences in splice site selection. Genes Dev. **7:** 407–418.

Weil, D., S. Blanchard, J. Kaplan, P. Guilford, F. Gibson *et al.*,

1995 Defective myosin VIIA gene responsible for Usher syndrome type 1B. Nature **374:** 60–61.

Weston, M. D., P. M. Kelley, L. D. Overbeck, M. Wagenaar, D. J. Orten *et al.*, 1996 Myosin VIIA mutation screening in 189 usher syndrome type 1 patients. Amer. J. Hum. Genet. **59:** 1074–1083.

Wu, X. F., B. Bowers, Q. Wei, B. Kocher and J. A. Hammer, 1997 Myosin V associates with melanosomes in mouse melanocytes—evidence that myosin V is an organelle motor. J. Cell Sci. **110:** 847–859.

Zhao, L. P., J. S. Koslovsky, J. Reinhard, M. Bahler, A. E. Witt *et al.*, 1996 Cloning and characterization of myr 6, an unconventional myosin of the dilute/myosin-V family. Proc. Natl. Acad. Sci. USA **93:** 10826–10831.

Communicating Editor: C. Kozak